Optimization of finite-length input volume holographic grating couplers illuminated by finite-width incident beams

Shun-Der Wu, Elias N. Glytsis, and Thomas K. Gaylord

A finite volume holographic grating coupler (VHGC) normally illuminated with various incident-beam profiles (such as a Gaussian beam, a flat cosine-squared beam, and an exponential-decay beam) with finite beam widths for input coupling is rigorously analyzed by use of the finite-difference frequency-domain method. The effects of the incident-beam width, the incident-beam position, the incident-beam profile, and the incident-beam angle of incidence on the input coupling efficiency are investigated. The optimum conditions for input coupling are determined. Both a VHGC embedded in the waveguide film region and a VHGC placed in the waveguide cover region are investigated. For a given finite VHGC, the input coupling efficiencies are strongly dependent on incident-beam widths, incident-beam positions, and incident-beam angles of incidence, but are only weakly dependent on incident-beam profiles. © 2005 Optical Society of America

OCIS codes: 050.0050, 050.1950, 050.1960, 050.7330, 260.2110.

1. Introduction

Grating couplers including both volume holographic gratings and surface-relief gratings can be used to couple an incident guided mode out of a waveguide (as an output grating coupler) or an incident beam into a waveguide (as an input grating coupler) for applications in guided-wave optical interconnects.[1–9] Relative to prism couplers and taper couplers, grating couplers provide some potential advantages including small weight, small size, and compatibility with integrated optoelectronics.[9] In addition to these advantages, grating couplers allow input coupling of diverging sources and focusing of outcoupled waves.[4,5]

For practical applications in high-data rate interconnections, input grating couplers have limited spatial apertures and are usually illuminated by finite-width beams such as Gaussian beams. Therefore, in contrast to output grating couplers, the coupling efficiency of input grating couplers depends not only on the grating geometry (grating lengths and grating periods) but also on the incident-beam properties (beam sizes, beam profiles, incident angles, and incident polarizations). In addition, as the incident beam is coupled into a guided mode by an input grating coupler, this guided mode will propagate in the waveguide and will be partially coupled out of the waveguide by the same grating. As a result, the input coupling efficiency will also depend on the incident beam's position on the grating coupler. On the other hand, in order to achieve a high coupling efficiency and a low optical cross talk in the system, preferential-order coupling is usually necessary. Volume holographic grating couplers (VHGCs), first proposed by Kogelnik and Sosnowski,[10] provide high coupling efficiency and high preferential-order coupling in integrated optics.[6,11,12] Furthermore, compared to the fabrication of surface-relief grating couplers (SRGCs) for high preferential-order coupling, the fabrication of VHGCs based on photopolymers eliminates all the chemical and etching steps, therefore reducing the fabrication complexity.

In order to analyze input grating couplers, Ogawa *et al.*[13] applied perturbation theory in conjunction with the coupled transmission line analysis to investigate the input coupling efficiency of an infinite SRGC illuminated by a plane wave with respect to

S.-D. Wu (gte782q@prism.gatech.edu) and T. K. Gaylord are with the Microelectronics Research Center, School of Electrical and Computer Engineering, Georgia Institute of Technology, Atlanta, Georgia 30332-1205. E. N. Glytsis is with the School of Electrical and Computer Engineering, National Technical University of Athens, Greece.

Received 19 November 2004; revised manuscript received 9 March 2005; accepted 21 March 2005.

0003-6935/05/214435-12$15.00/0

the grating periodicity, the grating depth, and the excitation condition. Neviere *et al.*[14–16] proposed a rigorous electromagnetic formalism deduced from Maxwell's equations to study the coupling resonances of an infinite SRGC illuminated by a plane wave as well as by a limited-extent incident beam. Dalgoutte and Wilkinson[17] applied the modified Born approximation and reciprocity theory to investigate the characteristics of a Gaussian beam launched into a single-mode waveguide and a multimode waveguide by use of SRGCs. Woldarczyk and Seshadri[18] also used perturbation theory to analyze an infinite SRGC with plane-wave incidence for both input and output coupling. Li and Gupta[19,20] applied the rigorous electromagnetic formalism developed by Neviere *et al.*[14–16] to investigate the input coupling efficiency with respect to angle detuning of an infinite SRGC illuminated by a Gaussian beam. Laval and coworkers[21,22] applied the same theory to study the optimized coupling of a SRGC illuminated by a Gaussian beam. Furthermore, Brazas and Li[23] also investigated the effects of the Gaussian beam size and of the length of a finite SRGC on the input coupling efficiency both experimentally and theoretically. Waldhäusl *et al.*[24] used the first-order perturbation theory, and Kwan and Taylor[25] developed a three-layer waveguide model to study the characteristics of input SRGCs with blazed profiles. Recently, Wang *et al.*[26] applied the finite-difference time-domain method to analyze both uniform and nonuniform input SRGCs for surface-normal coupling between fibers and waveguides. On the other hand, Ogawa and Chang[27] used perturbation theory to analyze both unslanted and slanted input VHGCs with infinite lengths illuminated by a plane wave with TE polarization.

However, to the authors' knowledge, there has been no rigorous analysis to determine simultaneously the effects of beam sizes, beam profiles, and incident-beam positions on the coupling efficiencies of input VHGCs with finite length that is comparable to the beam width and smaller than the intrinsic coupling length. Therefore, in this paper, the finite-difference frequency-domain (FDFD) method in conjunction with the uniaxial perfectly matched layer[12,28] (UPML) is used to analyze rigorously finite-length input VHGCs illuminated by finite-width beams. Only TE polarization is considered. In Section 2, the numerical method is briefly reviewed. In Section 3, numerical results for the coupling efficiencies of a finite-length input VHGC with respect to incident-beam sizes, incident-beam profiles, and incident-beam positions are presented. Furthermore, the effects of incident-beam angles of incidence on the input coupling efficiencies are also presented to show the angular sensitivities of input grating couplers. Finally, the primary results are summarized in Section 4.

2. Analysis Method

In this paper, an input VHGC in the waveguide film region as well as in the waveguide cover region

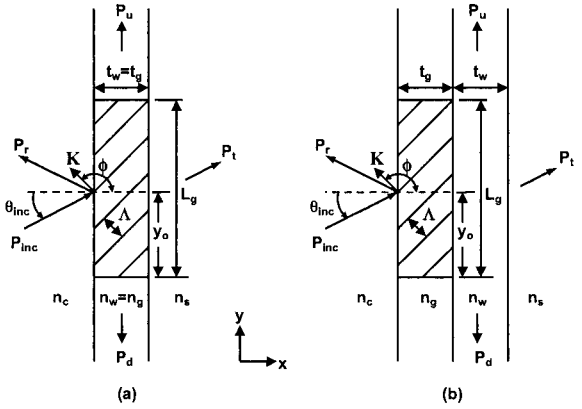

Fig. 1. Two basic configurations of waveguide input couplers comprised of a VHGC (a) in the waveguide film region and (b) in the waveguide cover region. The waveguide consists of a cover region with refractive index n_c, a film region with refractive index n_w, and a substrate region with refractive index n_s. The thickness of the waveguide film region is t_w. The volume holographic grating has a grating vector $\mathbf{K}$, a slant angle ϕ, a finite length L_g, and a thickness t_g. The average refractive index in the grating region is n_g. The incident beam with incident angle θ_{inc} and incident-beam position y_0 from the cover region is incident upon the grating. The power of the incident beam is P_{inc}. P_u, P_d, P_t, and P_r denote the upward-coupled power, the downward-coupled power, the transmitted power, and the reflected power, respectively.

[shown in Figs. 1(a) and 1(b), respectively] are analyzed by use of the FDFD method in conjunction with the UPML.[12,28] For both configurations, the waveguide consists of a glass substrate with refractive index n_s, a waveguide film layer with refractive index n_w and thickness t_w, and a cover layer with refractive index n_c. The average refractive index, the thickness, and the length of the holographic grating are n_g, t_g, and L_g, respectively. In addition, the grating vector $\mathbf{K}$ is defined as $\mathbf{K} = |\mathbf{K}|(\hat{x}\cos\phi + \hat{y}\sin\phi)$, where $|\mathbf{K}| = 2\pi/\Lambda$, Λ is the grating period, ϕ is the slant angle of the grating, and $\hat{x}$, $\hat{y}$ are the unit vectors along the x and y directions, respectively. The permittivity in the grating region can be written as

$$\begin{aligned}\epsilon &= \epsilon_0 \varepsilon(x, y) \\ &= \epsilon_0 \left\{ \varepsilon_0 + \sum_{p=1}^{\infty} \varepsilon_p{}^c \cos(p\mathbf{K}\cdot\mathbf{r}) + \sum_{p=1}^{\infty} \varepsilon_p{}^s \sin(p\mathbf{K}\cdot\mathbf{r}) \right\},\end{aligned} \tag{1}$$

where ϵ_0 is the permittivity of free space, $\varepsilon(x, y)$ is the dielectric constant, $\varepsilon_0 = n_g{}^2$ is the average dielectric constant, $\varepsilon_p{}^c$ and $\varepsilon_p{}^s$ are the pth harmonics of the dielectric constant (all in the grating region), and $\mathbf{r}$ is the position vector ($r = x\hat{x} + y\hat{y}$).

In order to investigate the effects of incident-beam angles and incident-beam positions on the coupling efficiencies of input VHGCs, a finite beam with incident angle θ_{inc} (measured from the normal of the grating interface in a counterclockwise direction) and incident-beam position y_0 is incident upon the grating from the cover region (Fig. 1). Furthermore, in order to study the effects of beam sizes and beam profiles on

the coupling efficiencies of input VHGCs, a Gaussian beam with beam width W, a flat cosine-squared beam (i.e., a quasi plane wave) with flat width W, and an exponential-decay beam (for modeling an incident beam produced by an output VHGC,[6,11,12] i.e., for grating-to-grating coupling) with decay width W are introduced in this research. The window function $g(y')$ can be represented for the Gaussian beam as

$$g(y') = \exp\left[\left(\frac{-y'}{W/2}\right)^2\right], \tag{2}$$

for the flat cosine-squared beam as

$$g(y') = \begin{cases} 1 & 0 \le |y'| \le \dfrac{W}{2} \\ \cos^2\left[\dfrac{|y'| - \dfrac{W}{2}}{2(D-W)}\,\pi\right] & \dfrac{W}{2} \le |y'| \le D - \dfrac{W}{2}, \\ 0 & D - \dfrac{W}{2} \le |y'| \le \infty \end{cases} \tag{3}$$

and for the exponential-decay beam as

$$g(y') = \begin{cases} \exp\left[-\alpha_l\left(y' - \dfrac{W}{2}\right)\right] & 0 \le |y'| \le \dfrac{W}{2} \\ \cos^2\left[\dfrac{|y'| - \dfrac{W}{2}}{2(D-W)}\,\pi\right] & \dfrac{W}{2} \le |y'| \le D - \dfrac{W}{2}, \\ 0 & D - \dfrac{W}{2} \le |y'| \le \infty \end{cases} \tag{4}$$

where α_l is the leakage parameter of a VHGC, which can be determined by use of the rigorous coupled-wave analysis in conjunction with leaky-mode (RCWA-LM) approach.[4,11] It is noted that the window function $g(y')$ for the exponential-decay beam [Eq. (4)] does not take into account the conjugate phase factor (as compared to the beam produced by an output VHGC). The corresponding configurations of the Gaussian, flat cosine-squared, and exponential-decay beams are summarized in Fig. 2. As a result, the incident beam for TE polarization can be represented by an electric field

$$\mathbf{E}_{\text{inc}} = g(y')\exp(-j\mathbf{k}\cdot\mathbf{r})\hat{z}\,, \tag{5}$$

where $\mathbf{k} = k_0 n_c(\hat{x}\ \cos\theta_{\text{inc}} + \hat{y}\ \sin\theta_{\text{inc}})$, $k_0 = 2\pi/\lambda_0$, and λ_0 is the free-space wavelength. In addition, as shown in Fig. 1, due to the grating vector lying in the plane of incidence, the configuration is the classical 2-D diffraction configuration. In this case, no TM diffracted wave is excited by a TE incident beam. Similarly, no TE diffracted wave is excited by a TM incident beam. Thus, for a TE incident wave, only TE–TE coupling is considered in this paper. TE–TM coupling only occurs for conical diffraction (i.e., the grating vector does not lie in the plane of incidence).

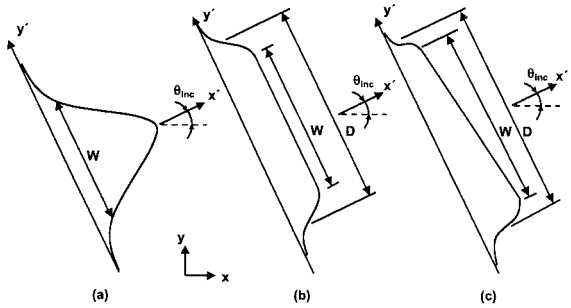

Fig. 2. Three finite-width incident beams: (a) a Gaussian beam with beam width W, (b) a flat cosine-squared beam (i.e., a quasi plane wave) with flat width W, and (c) an exponential-decay beam with decay width W. θ_{inc} is the incident angle of the incident beam.

A. Finite-Difference Frequency-Domain Method

The FDFD method uses the central difference approximation to discretize the Helmholtz equation.[12,28] For TE polarization ($\mathbf{E} = E_z\hat{z}$), the Helmholtz equation can be written as[12,28]

$$\nabla^2 E_z + \omega^2\mu\epsilon s E_z = 0, \tag{6}$$

where $s = 1 - j(\sigma/\omega\epsilon)$, μ is the permeability, ϵ is the permittivity, σ is the conductivity of the medium, and ω is the angular frequency. Of course μ, ϵ, and σ are in general position dependent. After discretizing the Helmholtz equation by using the central difference approximation, the end result of the FDFD formulation is a set of linear algebraic equations that can be written compactly as[12,28]

$$\bar{\bar{\mathbf{A}}}\mathbf{U} = \mathbf{b}, \tag{7}$$

where $\bar{\bar{\mathbf{A}}}$ is a coefficient matrix corresponding to the material properties and discretization parameters, $\mathbf{U}$ is a vector that contains the field values of $\mathbf{E}_z$ components for TE polarization, and $\mathbf{b}$ is a vector that represents the field of the incident beam. The detailed numerical considerations of the FDFD method including the performance of the UPML, and the effect of the mesh size on the numerical error can be found in Ref. 28.

B. Input Coupling Efficiencies of a Volume Holographic Grating Coupler

As shown in Fig. 1, a finite-width incident beam with power P_{inc} from the cover region is incident upon the input VHGC. The input VHGC is designed to couple the incident beam (assumed to be a plane wave) into the TE_0 mode of the waveguide (propagating in the upward direction) by use of the phase-matching condition for the first diffracted order. After applying the FDFD method to calculate the scattered field of $\mathbf{E}_z$ component for TE polarization, the modal decompo-

sition of guided fields is used to calculate the corresponding power coupled into the TE_m mode of the waveguide both in the upward direction, $P_{u,\,TE_m}$, and in the downward direction, $P_{d,\,TE_m}$. The modal decomposition for the power calculations of waveguide modes for TE polarization can be found in Appendix A. In addition, the plane-wave decomposition based on the fast Fourier transform is applied to calculate both the reflected power P_r and the transmitted power P_t.[28] In order to quantify the performance of an input VHGC, the input coupling efficiency of the TE_m mode $CE_{i,\,TE_m}$ is defined as

$$CE_{i,\,TE_m} = \frac{P_i}{P_{inc}} \times 100\%, \tag{8}$$

where P_{inc} is the incident power, and $P_i (i = u, d)$ is the diffracted power coupled in the upward direction or in the downward direction.

3. Numerical Results

The input VHGC analyzed in this paper is comprised of a fused-silica glass substrate of refractive index $n_s = 1.4567$ and of air as the cover region of refractive index $n_c = 1.0$. For an input VHGC in the waveguide film region [Fig. 1(a)], the waveguide material is assumed to be a photopolymer with refractive index $n_w = 1.5$ (e.g., DuPont's OmniDex613). On the other hand, for an input VHGC in the waveguide cover region [Fig. 1(b)] the waveguide material is assumed to be a polyimide with refractive index $n_w = 1.56$ (e.g., Ultradel9020D). In both cases, the grating material is a photopolymer with average dielectric constant $\varepsilon_0 = 2.25$ ($n_g = 1.5$) and modulation $\varepsilon_1^{\,c} = 0.06$ ($\Delta n_1 = 0.02$) (e.g., DuPont's OmniDex613).[29,30] The length of the finite VHGC is assumed to be $L_g = 50$ μm. In order to determine the optimum incident position, a normally incident beam (i.e., $\theta_{inc} = 0°$) of TE polarization with incident-beam position y_0 varying between $0.3L_g$ to $0.9L_g$ (i.e., $y_0 = 0.3L_g$, $0.4L_g$, $0.5L_g$, $0.6L_g$, $0.7L_g$, $0.8L_g$, and $0.9L_g$) from the cover region are considered. Furthermore, three different beam sizes of $W = L_g$, $0.5L_g$, and $0.25L_g$ for the Gaussian, flat cosine-squared, and exponential-decay beams are investigated. The free-space wavelength of the incident beam is assumed to be $\lambda_0 = 1.0$ μm.

A. Input Volume Holographic Grating Coupler in the Waveguide Film Region

For the configuration of an input VHGC in the waveguide film region [Fig. 1(a)], the thicknesses of the waveguide and the grating are $t_w = t_g = 1.8$ μm. The thickness t_w is designed to support a single TE mode in this waveguide. The propagation constant for the TE_0 mode is $\beta_{TE_0} = 9.335\ \mu m^{-1}$. Applying the standard phase-matching conditions between the normally incident beam and the TE_0 mode of the waveguide, the grating period and the slant angle of the grating are determined to be $\Lambda = 473.7$ nm and $\phi = 135.27°$, respectively. Furthermore, the corresponding leakage parameter calculated by using the RCWA-LM approach for this VHGC is $\alpha_l = 0.31 \times 10^{-2}\ \mu m^{-1}$.

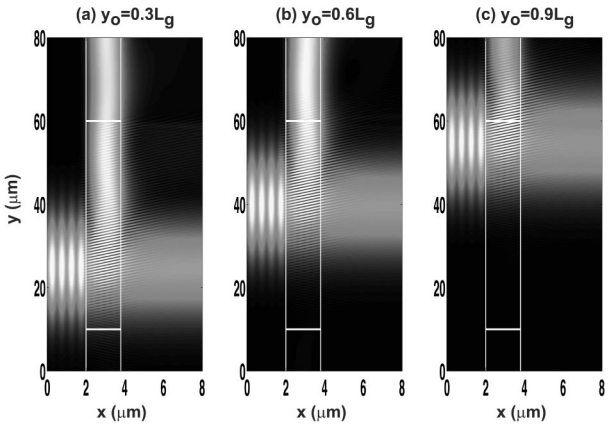

Fig. 3. Two-dimensional field-amplitude patterns of a finite input VHGC with $L_g = 50$ μm in the waveguide film region illuminated by a TE-polarized Gaussian beam with a beam width $W = 0.5L_g$ at the incident-beam position of (a) $y_0 = 0.3L_g$, (b) $y_0 = 0.6L_g$, and (c) $y_0 = 0.9L_g$.

1. Electric Fields

Figure 3 shows the amplitude patterns of the total electric field of a finite VHGC with $L_g = 50$ μm in the waveguide film region illuminated by a Gaussian beam with a beam width $W = 0.5L_g$ at three different incident positions ($y_0 = 0.3L_g$, $0.6L_g$, and $0.9L_g$). Dark areas indicate regions of lower field amplitude; the lighter areas indicate regions of higher field amplitude. In addition, both transmitted fields at $x = 8$ μm and input-coupled fields at $y = 80$ μm corresponding to Fig. 3 are also represented in Fig. 4.

As shown in Fig. 3(a) with the incident position $y_0 = 0.3L_g$, the Gaussian beam normally incident from the cover region is coupled into the TE_0 mode propagating in the waveguide, and then this guided mode is partially coupled out of the waveguide by the same VHGC from $y = 40$ μm to $y = 60$ μm [Fig. 4(a)]. This output-coupling effect results in the leakage of the guided mode from the waveguide and therefore degrades the performance of the input VHGC. However, as the incident-beam position is increased to $y_0 = 0.6L_g$, the output-coupling effect is small [Figs. 3(b) and 4(a)] because the larger value of y_0 corresponds to a shorter output-coupling length (i.e., less power of the guided mode will be coupled out of the waveguide for the larger y_0), and consequently, more of the power of the guided mode is retained in the waveguide. Therefore, as shown in Fig. 4(b), the amplitude of the input-coupled field of $y_0 = 0.6L_g$ is higher than that of $y_0 = 0.3L_g$. In other words, the input coupling efficiency increases as the incident-beam position increases from $y_0 = 0.3L_g$ to $y_0 = 0.6L_g$. As the incident-beam position increases further, for example, $y_0 = 0.9L_g$, although the output-coupling effect of $y_0 = 0.9L_g$ is much smaller than those of $y_0 = 0.3L_g$ and $y_0 = 0.6L_g$ [Fig. 4(a)], some of the incident beam initially falls outside the VHGC

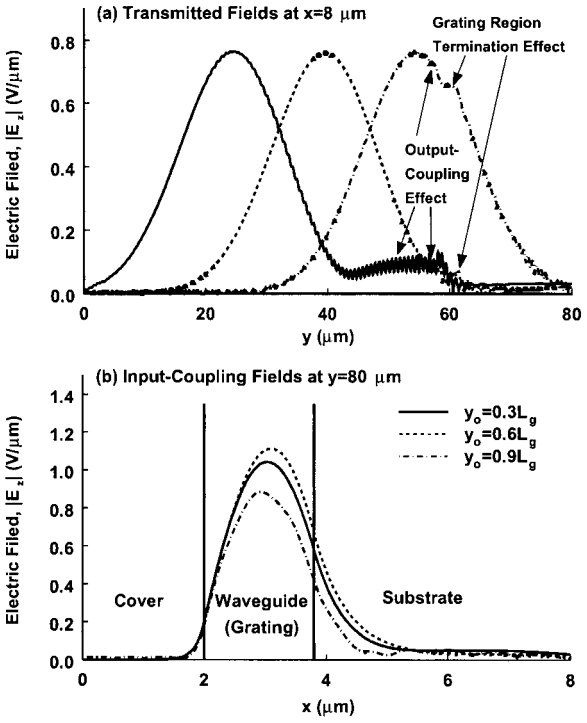

Fig. 4. Field profiles corresponding to Fig. 3 for (a) the transmitted field at $x = 8\ \mu m$ and (b) the input-coupled field at $y = 80\ \mu m$.

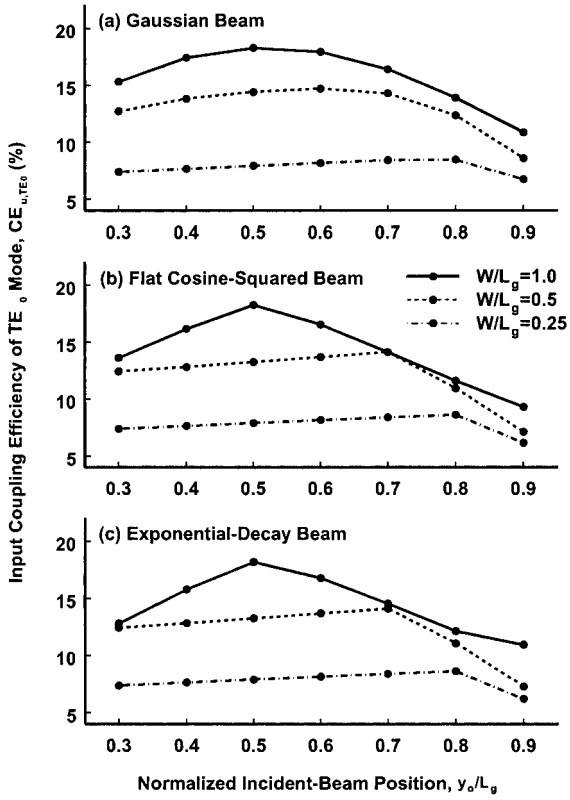

Fig. 5. Input coupling efficiencies of the TE_0 mode in the upward direction as functions of y_0/L_g and W/L_g for a finite input VHGC with $L_g = 50\ \mu m$ in the waveguide film region illuminated by (a) a Gaussian beam, (b) a flat cosine-squared beam, and (c) an exponential-decay beam.

and is transmitted through the waveguide without being diffracted [Fig. 3(c)]. This grating region termination effect can be seen in Fig. 4(a). Therefore, the amplitude of the input-coupled field decreases as the incident-beam position increases to $y_0 = 0.9L_g$ [Fig. 4(b)]. In summary, for a finite input VHGC in the waveguide film region, there is an optimum incident position for a finite incident-beam to obtain the maximum coupling efficiency.

2. Optimization of Input-Coupling Efficiencies

Figure 5 shows the numerical results of input coupling efficiencies of the TE_0 mode in the upward direction ($CE_{u,\,TE_0}$) as a function of normalized incident-beam positions with various incident-beam widths and different incident-beam profiles for a VHGC in the waveguide film region. It is noted that the input coupling efficiencies of the TE_0 mode in the downward direction ($CE_{d,\,TE_0}$) for all cases of input VHGCs in the waveguide film region treated in this paper are smaller than 0.02%. As shown in Fig. 5(a), the optimum incident positions, $y_{0,\,opt}$, and the corresponding input coupling efficiencies, $CE_{u,\,TE_0}$, of Gaussian beams with beam widths $W = L_g$, $0.5L_g$, and $0.25L_g$ are $y_{0,\,opt} = 0.5L_g$, $0.6L_g$, and $0.8L_g$ and $CE_{u,\,TE_0} = 18.29\%$, 14.71%, and 8.46%, respectively. As is discussed in Subsection 3.A.1, for $y_0 < y_{0,\,opt}$, the input coupling efficiency increases as the incident-beam position increases because the output-coupling effect decreases. On the other hand, for $y_0 > y_{0,\,opt}$, the input coupling efficiency decreases as the incident-beam position increases because the grating region termination effect increases. Furthermore, the input coupling efficiency (at the optimum coupling condition) decreases as the incident-beam width decreases because narrower beams are spread more in wave-vector space, resulting in significant deviations from the phase-matching condition of the first diffracted order, and thus, smaller coupling efficiencies. The characteristics of input coupling efficiencies with respect to the incident-beam position (y_0/L_g) and the incident-beam width (W/L_g) for a finite input VHGC illuminated by a flat cosine-squared beam [Fig. 5(b)] and by an exponential-decay beam [Fig. 5(c)] are similar to those of a finite input VHGC illuminated by a Gaussian beam. Comparing Figs. 5(a), 5(b), and 5(c), the beam profiles do not significantly affect the performance of a finite input VHGC.

The optimum incident positions and the corresponding coupling efficiencies in the upward direction ($CE_{u,\,TE_0}$) of a finite input VHGC in the waveguide film region are summarized in Table 1. As shown in Table 1, as the incident-beam widths decrease from $W = L_g$ to $W = 0.5L_g$, the optimum incident positions increase from $y_{0,\,opt} = 0.5L_g$ to $y_{0,\,opt} = 0.6L_g$ for the Gaussian beam and to $y_{0,\,opt} = 0.7L_g$ for both the flat cosine-squared beam and the exponential-decay beam. However, as the incident-

Table 1. Optimizations for the Coupling of Finite Beams into a Waveguide via a VHGC of Length $L_g = 50$ μm in a Waveguide Film Region

Beam Profiles	Beam Width W/L_g	Optimizations for Coupling into the TE_0 Mode: Optimum Incident Position $y_{0,\,opt}/L_g$	Optimizations for Coupling into the TE_0 Mode: Input Coupling Efficiency $CE_{u,\,TE_0}$(%)
Gaussian	1.0	0.5	18.29
	0.5	0.6	14.71
	0.25	0.8	8.46
Flat cosine-squared	1.0	0.5	18.30
	0.5	0.7	14.15
	0.25	0.8	8.65
Exponential-decay	1.0	0.5	18.19
	0.5	0.7	14.13
	0.25	0.8	8.65

beam width decreases further (i.e., $W = 0.25L_g$), the optimum incident-beam positions for all beam profiles increase to $y_{0,\,opt} = 0.8L_g$. Consequently, for a given beam profile, the optimum incident position $y_{0,\,opt}$ shifts to the end of the VHGC as the incident-beam width decreases. However, the optimum incident position of a finite input VHGC is weakly dependent on the beam profiles. Since the conjugate phase factors of the window functions for the exponential-decay beams are neglected (as compared to the case of an output VHGC), the coupling efficiencies of the exponential-decay beams are not always better than those of the Gaussian beams and the flat cosine-squared beams. Finally, it is worth mentioning that the output-coupling efficiency of this same VHGC device is 25.47% as the TE_0 mode is incident and light is coupled out of the waveguide into the cover.

3. Angular Sensitivities

In order to study the effect of incident angles on the input coupling efficiency of a finite input VHGC in the waveguide film region, a Gaussian beam with beam width $W = 0.5L_g$ is incident upon the VHGC at its optimum incident position $y_{0,\,opt} = 0.6L_g$ (Table 1). The incident angle varies from $-2°$ to $2.5°$.

Figure 6 shows the input coupling efficiency to the TE_0 mode in the upward direction as a function of incident angles. As shown in Fig. 6, the maximum input coupling efficiency is $CE_{u,\,TE_0} = 16.29\%$ at an incident angle of $\theta_{inc} = 0.34°$, which is slightly off the designed value of $\theta_{inc} = 0°$ (i.e., normal incidence). The reason for the difference between the optimum incident angle and the designed incident angle is that the grating period and the slant angle are designed based on the propagation constant of a waveguide without consideration of the grating modulation. A similar deviation can also be observed in the case of output VHGCs.[12] In addition, the full-width half-maximum (FWHM) is $FWHM_{TE_0} = 1.77°$ for a Gaussian beam with a beam width $W = 0.5L_g$.

B. Input Volume Holographic Grating Coupler in the Waveguide Cover

For the configuration of an input VHGC in the waveguide cover region [as shown in Fig. 1(b)], the thicknesses of the waveguide film and the grating are $t_w = 0.4$ μm and $t_g = 6.0$ μm, respectively. Based on this waveguide structure, there are five TE modes. The propagation constants of the first two TE modes are $\beta_{TE_0} = 9.456\ \mu m^{-1}$ (confined in the film region) and $\beta_{TE_1} = 9.407\ \mu m^{-1}$ (confined in the film-grating region). Similarly, using the standard phase-matching conditions, the designed grating period and the slant angle of the input VHGC in the waveguide cover region are $\Lambda = 470.6$ nm and $\phi = 134.91°$, respectively, to couple the normally incident beam into the TE_0 mode of the waveguide. Moreover, the corresponding leakage parameter determined by using the RCWA-LM approach for this VHGC is $\alpha_l = 0.28 \times 10^{-2}\ \mu m^{-1}$.

1. Electric Fields

The amplitude patterns of the total electric field of a finite VHGC with $L_g = 50$ μm in the waveguide cover region illuminated by a Gaussian beam with beam

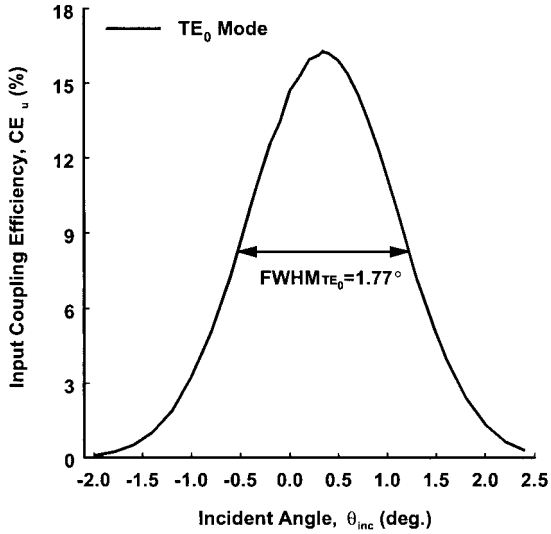

Fig. 6. Angular sensitivities of the TE_0 mode for a finite input VHGC in the waveguide film region illuminated by a Gaussian beam with a beam width $W = 0.5L_g$ at its optimum incident-beam position of $y_{0,\,opt} = 0.6L_g$.

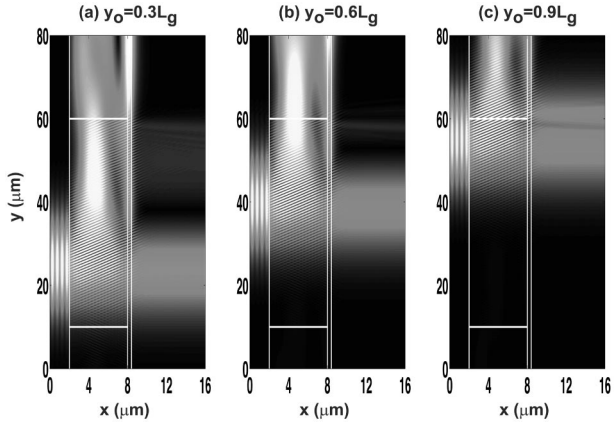

Fig. 7. Two-dimensional field-amplitude patterns of a finite input VHGC with $L_g = 50$ μm in the waveguide cover region illuminated by a TE-polarized Gaussian beam with a beam width $W = 0.5L_g$ at the incident-beam position of (a) $y_0 = 0.3L_g$, (b) $y_0 = 0.6L_g$, and (c) $y_0 = 0.9L_g$.

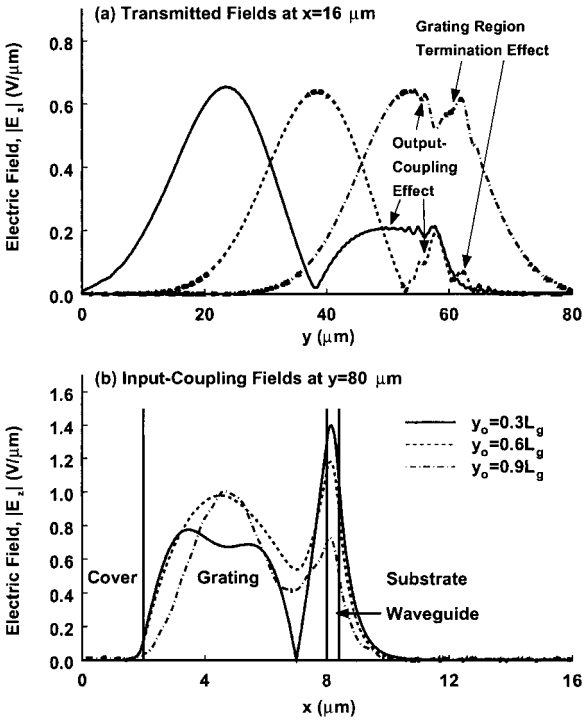

Fig. 8. Field profiles corresponding to Fig. 6 for (a) the transmitted field at $x = 16$ μm and (b) the input-coupled field at $y = 80$ μm.

width $W = 0.5L_g$ at three different incident positions ($y_0 = 0.3L_g$, $0.6L_g$, and $0.9L_g$) are shown in Fig. 7. Again, dark areas indicate regions of lower field amplitude; the lighter areas indicate regions of higher field amplitude. In addition, both transmitted fields at $x = 16$ μm and input-coupled fields at $y = 80$ μm corresponding to Fig. 7 are also represented in Fig. 8.

As shown in Figs. 7 and 8(a), the characteristics of the output-coupling effect (causing the leakage of guided modes) and grating region termination effect (resulting in incomplete interaction between the incident beam and the finite VHGC) of a finite input VHGC in the waveguide cover region are similar to those of a finite input VHGC in the waveguide film region. Therefore, there is also an optimum incident position for a finite incident beam for a finite input VHGC in the waveguide cover region. The optimization of an input VHGC in the waveguide cover region is discussed in Subsection 3.B.2. However, in contrast to the configuration of a finite input VHGC in the waveguide film region [Figs. 3 and 4(b)], another interesting phenomenon for the case of a finite input VHGC in the waveguide cover region is that an additional mode (TE_1) is excited. As shown in Figs. 7 and 8(b), in addition to the fundamental TE_0 mode (confined in the film layer), the TE_1 mode (confined in the grating-film layer) is excited by the input VHGC.

2. Optimization of Input Coupling Efficiencies

The numerical results for the input coupling efficiencies (in the upward direction) of both the TE_0 mode ($CE_{u,\,TE_0}$) and the TE_1 mode ($CE_{u,\,TE_1}$) as a function of y_0/L_g with various incident-beam widths and different beam profiles for a VHGC in the waveguide cover region are represented in Figs. 9 and 10, respectively. It is noted that for all cases of input VHGCs in the waveguide cover region treated in this paper, the input coupling efficiencies (in the upward direction) of the TE_2 mode ($CE_{u,\,TE_2}$), the TE_3 mode ($CE_{u,\,TE_3}$), and the TE_4 mode ($CE_{u,\,TE_4}$) are smaller than 1.0%, 2.0%, and 0.005%, respectively. Furthermore, the input coupling efficiencies for all guided modes in the downward direction are smaller than 0.06%. The optimum incident positions ($y_{0,\,opt}$) and the corresponding coupling efficiencies (in the upward direction) for both the TE_0 mode and the TE_1 mode of a finite input VHGC in the waveguide cover region are summarized in Table 2. Similar to an input VHGC in the waveguide film region, the coupling efficiencies of the exponential-decay beams are not always better than those of the Gaussian beams and the flat cosine-squared beams due to the lack of the conjugate phase factors of the window functions for the exponential-decay beams (compared to the case of an output VHGC).

As shown in Figs. 9 and 10, similar to the case of a finite input VHGC in the waveguide film region (Fig. 5), the input coupling efficiency is strongly dependent on the incident-beam width as well as the incident-beam position, but is only weakly dependent on the incident-beam profile. On the other hand, as shown in Table 2, the optimum incident positions of $y_{0,\,opt}$ for both the TE_0 mode and the TE_1 mode shift to the end of the VHGC as the incident-beam width decreases. Furthermore, the corresponding input coupling efficiencies for both the TE_0 mode and the TE_1 mode (at the optimum coupling condition) decrease as the incident-beam width decreases. However, the incident-beam profile does not significantly affect the

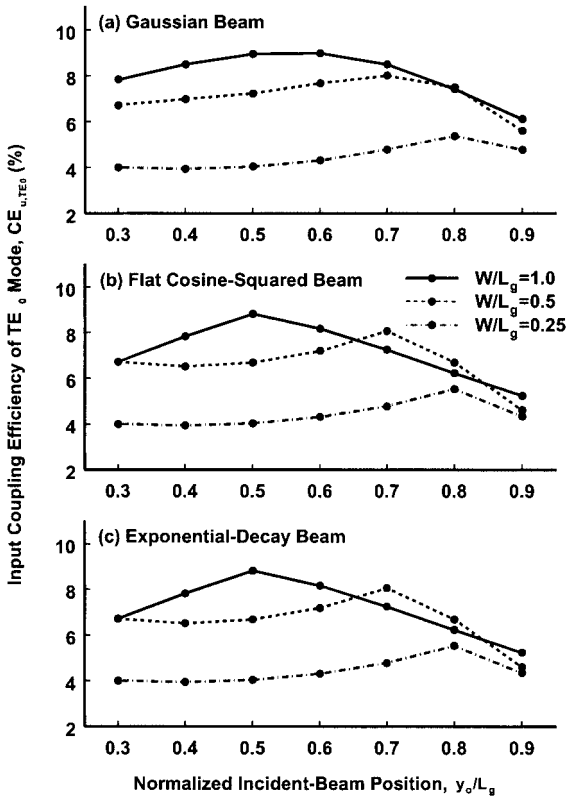

Fig. 9. Input coupling efficiencies of the TE_0 mode in the upward direction as functions of y_0/L_g and W/L_g for a finite input VHGC with $L_g = 50$ μm in the waveguide cover region illuminated by (a) a Gaussian beam, (b) a flat cosine-squared beam, and (c) an exponential-decay beam.

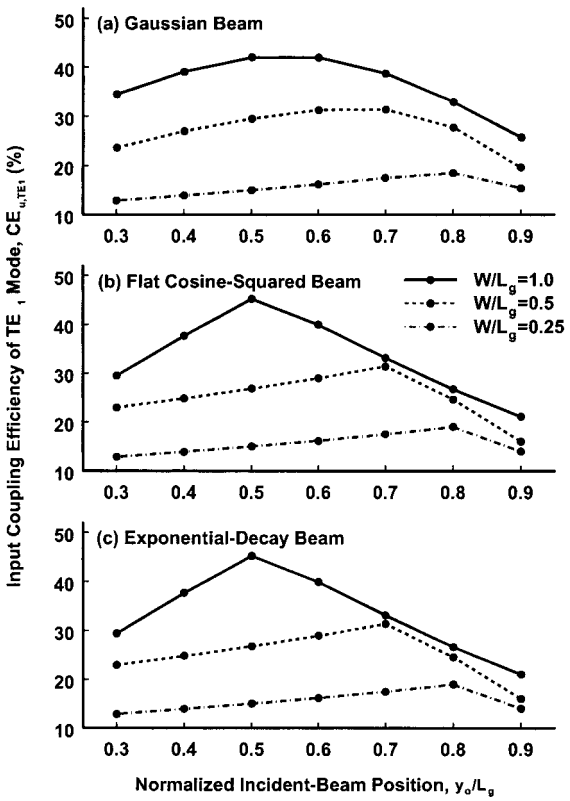

Fig. 10. Input coupling efficiencies of the TE_1 mode in the upward direction as functions of y_0/L_g and W/L_g for a finite input VHGC with $L_g = 50$ μm in the waveguide cover region illuminated by (a) a Gaussian beam, (b) a flat cosine-squared beam, and (c) an exponential-decay beam.

optimization of a finite input VHGC in the waveguide cover region.

Comparing Figs. 9 and 10, although the input VHGC is designed to couple a normally incident beam into the TE_0 mode of the waveguide based on the phase-matching condition for the first diffracted order, the input coupling efficiencies of the TE_1 mode are much higher than those of the TE_0 mode. For example, for a VHGC in the waveguide cover region illuminated by a Gaussian beam with $W = 0.5L_g$ at the optimum incident position of $y_0 = 0.7L_g$, the input coupling efficiencies for the TE_0 mode and the TE_1 mode are $CE_{u,\,TE_0} = 8.00\%$ and $CE_{u,\,TE_1} = 31.38\%$.

In addition, the output-coupling efficiencies of this VHGC device in the waveguide cover region (i.e., the guided modes are incident on the VHGC and are coupled out of the waveguide into the cover) are 16.48% and 48.98% for the TE_0-mode incidence and the TE_1-mode incidence, respectively. In contrast to the TE_0 mode that is confined primarily in the film layer, the TE_1 mode is confined primarily in the grating layer, and therefore, the interaction between the TE_1 mode and the VHGC is stronger than the interaction between the TE_0 mode and the VHGC. As a result, the output-coupling efficiency for TE_1-mode incidence is higher than that for TE_0-mode incidence, even though the grating is based on the phase-matching condition for the TE_0 mode.

3. *Angular Sensitivities*

Similar to the case of a finite input VHGC in the waveguide film region, a finite input VHGC in the waveguide cover region illuminated by a Gaussian beam with beam width $W = 0.5L_g$ for a range of incident angles is analyzed to study its angular sensitivity. The incident position is selected as the optimum incident position $y_{0,\,opt} = 0.7L_g$ (Table 2), and the incident angle varies from $-2.0°$ to $2.5°$.

Figure 11 shows the input coupling efficiencies for both TE_0 and TE_1 modes in the upward direction as a function of incident angles. As shown in Fig. 11, the maximum input coupling efficiency of the TE_0 mode is $CE_{u,\,TE_0} = 9.22\%$, and the corresponding optimum incident angle is $\theta_{inc} = 0.39°$. Similar to the case of an input VHGC in the waveguide film region, the optimum incident angle of the TE_0 mode slightly shifts from the designed value of $\theta_{inc} = 0°$. The reason for this deviation is the same as that previously described in Subsection 3.A.3. However, the maximum input coupling efficiency of the TE_1 mode is $CE_{u,\,TE_1} = 31.67\%$ when the incident angle is $\theta_{inc} = -0.10°$, which is smaller than that of the TE_0 mode. This result is expected because the propagation constant

Table 2. Optimizations for the Coupling of Finite Beams into a Waveguide via a VHGC of Length L_g = 50 μm in a Waveguide Cover Region

Beam Profiles	Beam Width W/L_g	Optimizations for Coupling into the TE_0 Mode: Optimum Incident Position $y_{0,\,opt}/L_g$	Optimizations for Coupling into the TE_0 Mode: Input Coupling Efficiency $CE_{u,\,TE_0}$(%)
Gaussian	1.0	0.6	8.98
	0.5	0.7	8.00
	0.25	0.8	5.37
Flat cosine-squared	1.0	0.5	8.83
	0.5	0.7	8.07
	0.25	0.8	5.53
Exponential-decay	1.0	0.5	8.83
	0.5	0.7	8.07
	0.25	0.8	5.53

Beam Profiles	Beam Width W/L_g	Optimizations for Coupling into the TE_1 Mode: Optimum Incident Position $y_{0,\,opt}/L_g$	Optimizations for Coupling into the TE_1 Mode: Input Coupling Efficiency $CE_{u,\,TE_1}$(%)
Gaussian	1.0	0.5	42.02
	0.5	0.7	31.38
	0.25	0.8	18.57
Flat cosine-squared	1.0	0.5	42.27
	0.5	0.7	31.43
	0.25	0.8	19.02
Exponential-decay	1.0	0.5	42.27
	0.5	0.7	31.43
	0.25	0.8	19.02

of the TE_1 mode is smaller than that of the TE_0 mode. In addition, the values of FWHM for both the TE_0 mode and the TE_1 mode are $FWHM_{TE_0}$ = 1.88° and $FWHM_{TE_1}$ = 1.91°, respectively, for a Gaussian beam with a beam width $W = 0.5L_g$.

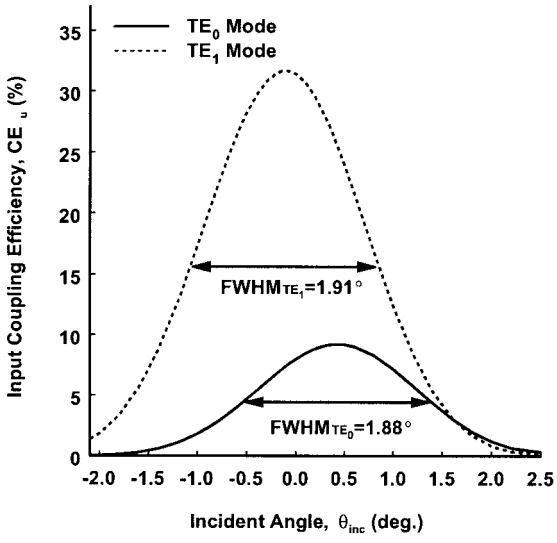

Fig. 11. Angular sensitivities of both TE_0 and TE_1 modes for a finite input VHGC in the waveguide cover region illuminated by a Gaussian beam with a beam width $W = 0.5L_g$ at its optimum incident-beam position of $y_{0,\,opt} = 0.7L_g$.

4. Summary and Discussion

The effects of the incident-beam width, the incident-beam position, the incident-beam profile, and the incident-beam angle of incidence on the input coupling efficiency of a finite input VHGC have been investigated for TE incident polarization by use of the FDFD rigorous electromagnetic method. Two configurations of an input VHGC embedded in the waveguide film region as well as an input VHGC placed in the waveguide cover region were examined.

For both configurations, the preceding numerical analysis has shown that the incident-beam width, the incident-beam position, and the incident angle can dramatically affect the input coupling efficiency. In general, for a given VHGC, the input coupling efficiency decreases as the incident-beam width decreases because a narrower beam corresponds to a broader spectrum of spatial frequencies, resulting in a significant deviation from the phase-matching condition for the first diffracted order, and thus, a smaller coupling efficiency. For the effects of incident-beam positions on input coupling efficiencies, depending on both the output-coupling effect and the grating region termination effect, an optimum incident position $y_{0,\,opt}$, which is strongly dependent on the incident-beam width, for a given beam has been obtained. For example, the optimum incident positions of a VHGC in the waveguide film region illuminated by a Gaussian beam are $y_{0,\,opt} = 0.5L_g$, $0.6L_g$, and

$0.8L_g$ for incident-beam widths of $W = L_g$, $0.5L_g$ and $W = 0.25L_g$, respectively. Similar results for the optimization of a flat cosine-squared beam and an exponential-decay beam can also be observed. In summary, the optimum incident-beam position shifts to the end of a VHGC as the incident beam width decreases. On the other hand, the beam profile does not dramatically affect either the input coupling efficiency or the optimization of input coupling. However, the input coupling efficiencies of the exponential-decay beams are not always better than those of the Gaussian beams and the flat cosine-squared beams due to the lack of the conjugate phase factors of the exponential-decay beams (compared to the output coupler phase factors). Furthermore, the optimum incident angles of the TE_0 mode by an input VHGC both in the waveguide film region and in the waveguide cover region shift from the designed value of $\theta_{inc} = 0°$ to $\theta_{inc} = 0.34°$ and $\theta_{inc} = 0.39°$, respectively.

It is also noted that the optimum efficiencies for coupling into the TE_0 mode of an input VHGC both in the waveguide film region and in the waveguide cover region are about 18% and 10%, respectively. The reason for the small coupling efficiencies is that the VHGC is only 50 μm long. However, a high input coupling efficiency can be realized by increasing the length of the VHGC and the width of the incident beam based on the optimum incident-beam position and the optimum incident-beam angle of incidence. For example, the coupling efficiency of an input VHGC with $L_g = 250$ μm in the waveguide film region can achieve up to $CE_{u,\,TE_0} = 65.15\%$ for a Gaussian beam incidence with $W = L_g$, $y_0 = 0.5L_g$, and $\theta_{inc} = 0.34°$. It is worth mentioning that for the same configuration of an input VHGC the coupling efficiency for the same Gaussian beam with $\theta_{inc} = 0°$ (i.e. normal incidence) is only $CE_{u,\,TE_0} = 0.51\%$, which is much smaller than that for $\theta_{inc} = 0.34°$. This result is expected because the wider incident beam results in narrower angular selectivity of the input VHGC. Therefore, the input coupling efficiency will dramatically decrease as the incident angle is deviated from the optimum incident angle for a wider incident beam.

In addition, the FDFD results show that there is a higher-order waveguide mode excitation in the configuration of an input VHGC in the waveguide cover region. An interesting observation is that the input coupling efficiency of the TE_1 mode is much higher than that of the TE_0 mode, even though the grating phase-matching condition used corresponds to the TE_0 mode. This is due to the modal intensity profile of the TE_1 mode in the grating layer being much larger than that of the TE_0 mode in the grating layer. As expected, the modal intensity profile of the TE_0 mode is relatively small in the grating layer. By comparison, it is much larger in the waveguide layer, but the resulting coupling is relatively weak due to the small overlap of the TE_0 mode with the grating layer in spite of the phase-matching condition being satisfied for the TE_0 mode. This result is consistent with the case of this device used as an output VHGC (Subsection 3.B.2). Furthermore, the optimum incident angle of an input VHGC in the waveguide cover region for coupling into the TE_1 mode is $\theta_{inc} = -0.10°$.

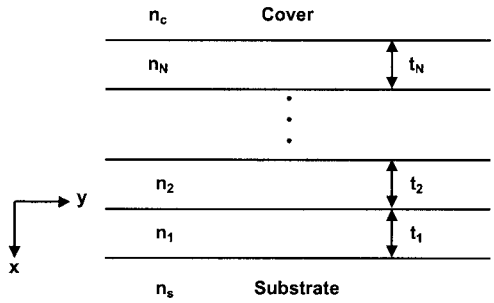

Fig. 12. Configuration of a multilayer slab waveguide consisting of a stack of N layers with finite thickness bounded on either side by two semi-infinite media, denoted as a substrate with refractive index n_s and a cover with refractive index n_c. The thickness and the refractive index of the ith layer are t_i and n_i, respectively.

Appendix A: Modal Decomposition for Power in Waveguide Modes

A multilayer slab waveguide, shown in Fig. 12, consists of a stack of N layers with finite thickness bounded on either side by two semi-infinite media, denoted as a substrate with refractive index n_s and a cover with refractive index n_c. The thickness and the refractive index of the ith layer are t_i and n_i, respectively. The slab waveguide is infinite in extent in the y–z plane, but finite in the x direction.

In order to calculate the power in the guided modes supported by the multilayer slab waveguide, modal decomposition is applied. First, it is assumed that the polarization is TE (electric field along the z axis). Based on the modal decomposition, any field profile along the transverse direction (i.e., along the x axis), $\mathscr{E}_z(x)$, of the slab waveguide can be expressed in terms of guided modes and radiation modes as

$$\mathscr{E}_z(x) = \sum_m a_m \mathscr{E}_{mz}(x) + \int_\beta q(\beta)\, \mathscr{E}_z(x,\ \beta)\mathrm{d}\beta, \quad \text{(A1)}$$

where $\mathscr{E}_{mz}(x)$ and $\mathscr{E}_z(x, \beta)$ represent the field profiles of the TE_m guided mode and the radiation mode, respectively, and a_m and $q(\beta)$ are unknown coefficients. Therefore, the electric field of the waveguide $E_z(x)$ can be represented as

$$E_z(x) = \sum_m a_m \mathscr{E}_{mz}(x)\exp(-j\beta_m y) + \int_\beta q(\beta)\, \mathscr{E}_z(x,\ \beta) \times \exp(-j\beta y)\mathrm{d}\beta, \quad \text{(A2)}$$

where β_m and β are the propagation constants of the mth guided mode and the radiation mode, respectively. In addition, it is well known that the modes of the waveguide form a basis, and they satisfy the orthogonality conditions of the form

$$\langle \mathcal{E}_{mz}(x),\ \mathcal{E}_{nz}(x)\rangle = \frac{\beta_m}{2\omega\mu_0}\int_{-\infty}^{\beta_m} \mathcal{E}_{mz}(x)\,\mathcal{E}_{nz}^{*}(x)\mathrm{d}x = \mathcal{P}_{\mathrm{TE}_m}\delta_{m,n}, \quad \text{(A3)}$$

where ω is the angular frequency, μ_0 is the permeability of free space, $\mathcal{P}_{\mathrm{TE}_m}$ the normalized power of mth guided mode for TE polarization (per unit length along the z axis), and $\delta_{m,n}$ is the Kronecker's symbol. It is noted that the orthogonality condition holds for radiation modes as well as between guided modes and radiation modes. Multiplying by $(\beta_n/2\omega\mu_0)\,\mathcal{E}_{nz}^{*}(x)$ both sides of Eq. (A1) and applying the orthogonality condition, the unknown coefficients of a_m and $q(\beta)$ can be expressed as

$$a_m = \frac{1}{\mathcal{P}_{\mathrm{TE}_m}}\langle \mathcal{E}_z(x),\ \mathcal{E}_{mz}(x)\rangle = \frac{1}{\mathcal{P}_{\mathrm{TE}_m}}\frac{\beta_m}{2\omega\mu_0}\int_{-\infty}^{\infty} \mathcal{E}_z(x)\,\mathcal{E}_{mz}^{*}(x)\mathrm{d}x, \quad \text{(A4)}$$

$$q(\beta) = \frac{1}{\mathcal{P}_{\mathrm{TE}_\beta}}\langle \mathcal{E}_z(x),\ \mathcal{E}_z(x,\ \beta)\rangle = \frac{1}{\mathcal{P}_{\mathrm{TE}_\beta}}\frac{\beta}{2\omega\mu_0}\int_{-\infty}^{\infty} \mathcal{E}_z(x)\,\mathcal{E}_z^{*}(x,\ \beta)\mathrm{d}x. \quad \text{(A5)}$$

As a result, the corresponding power for TE polarization in a slab waveguide can be expressed as

$$P_{\mathrm{TE}} = \sum_m |a_m|^2\mathcal{P}_{\mathrm{TE}_m} + \int_\beta |q(\beta)|^2\mathcal{P}_{\mathrm{TE}_\beta}\mathrm{d}\beta. \quad \text{(A6)}$$

In other words, the guided power in the TE_m mode, P_{TE_m}, is given by

$$P_{\mathrm{TE}_m} = |a_m|^2\mathcal{P}_{\mathrm{TE}_m}. \quad \text{(A7)}$$

This research was supported by the State of Georgia Yamacraw Project. Elias N. Glytsis was partially supported by the National Science Foundation grant ERC-94-02723.

References

1. S. H. Song and E. H. Lee, "Focusing-grating-coupler arrays for uniform and efficient signal distribution in a backboard optical interconnect," Appl. Opt. **34,** 5913–5919 (1995).
2. Q. Xing, S. Ura, T. Suhara, and H. Nishihara, "Contra-directional coupling between stacked waveguides using grating couplers," Opt. Commun. **144,** 180–182 (1997).
3. Q. Huang and P. R. Ashley, "Holographic Bragg grating input–output couplers for polymer waveguides at an 850-nm wavelength," Appl. Opt. **36,** 1198–1203 (1997).
4. S. M. Schultz, E. N. Glytsis, and T. K. Gaylord, "Design of a high-efficiency volume grating couplers for line focusing," Appl. Opt. **37,** 2278–2287 (1998).
5. S. M. Schultz, E. N. Glytsis, and T. K. Gaylord, "Volume grating preferential-order focusing waveguide coupler," Opt. Lett. **24,** 1708–1710 (1999).
6. S. M. Schultz, E. N. Glytsis, and T. K. Gaylord, "Design, fabrication, and performance of preferential-order volume grating waveguide couplers," Appl. Opt. **39,** 1223–1232 (2000).
7. R. T. Chen, L. Lin, C. Choi, Y. J. Liu, B. Bihari, L. Wu, S. Tang, R. Wickman, B. Picor, M. K. Hibbs-Brenner, J. Bristow, and Y. S. Liu, "Fully embedded board-level guided-wave optoelectronic interconnects," Proc. IEEE **88,** 780–793 (2000).
8. T. Tanaka, H. Takahashi, Y. Hibino, T. Hashimoto, A. Himeno, Y. Yamada, and Y. Tohmori, "Hybrid external cavity lasers composed of spot-size converter integrated LDs and UV written Bragg grating in a planar lightwave circuit on Si," IEICE Trans. Electron. **E83-C,** 875–883 (2000).
9. S. M. Schultz, "High efficiency volume holographic grating coupler," Ph.D. dissertation (Georgia Institute of Technology, 1999).
10. H. Kogelnik and T. P. Sosnowski, "Holographic thin film couplers," Bell Syst. Tech. J. **49,** 1602–1608 (1970).
11. R. A. Villalaz, E. N. Glytsis, and T. K. Gaylord, "Volume grating couplers: polarization and loss effect," Appl. Opt. **41,** 5223–5229 (2002).
12. S.-D. Wu and E. N. Glytsis, "Volume holographic grating couplers: rigorous analysis using the finite-difference frequency-domain method," Appl. Opt. **43,** 1009–1023 (2004).
13. K. Ogawa, W. S. C. Chang, B. L. Sopori, and F. J. Rosenbaum, "A theoretical analysis of etched grating couplers for integrated optics," IEEE J. Quantum Electron. **9,** 29–42 (1973).
14. M. Neviere, R. Petit, and M. Cadilhac, "About the theory of optical grating coupler-waveguide system," Opt. Commun. **8,** 113–117 (1973).
15. M. Neviere, P. Vincent, R. Petit, and M. Cadilhac, "Systematic study of resonances of holographic thin film couplers," Opt. Commun. **9,** 48–53 (1973).
16. M. Neviere, P. Vincent, R. Petit, and M. Cadilhac, "Determination of the coupling coefficient of a holographic thin film coupler," Opt. Commun. **9,** 240–245 (1973).
17. D. G. Dalgoutte and C. D. W. Wilkinson, "Thin grating couplers for integrated optics: an experimental and theoretical study," Appl. Opt. **14,** 2983–2998 (1975).
18. M. T. Woldarczyk and S. R. Seshadri, "Analysis of grating couplers in planar waveguides for waves at oblique incidence," J. Opt. Soc. Am. A **2,** 171–185 (1985).
19. L. Li and M. C. Gupta, "Effects of beam focusing on the efficiency of planar waveguide grating couplers," Appl. Opt. **29,** 5320–5325 (1990).
20. M. C. Gupta and L. Li, "Effect of beam defocus on the efficiency of planar waveguide grating couplers," Appl. Opt. **30,** 4402–4405 (1991).
21. D. Pascal, R. Orobtchouk, A. Layadi, A. Koster, and S. Laval, "Optimized coupling of a Gaussian beam into an optical waveguide with a grating coupler: comparison of experimental and theoretical results," Appl. Opt. **36,** 2443–2447 (1997).
22. R. Orobtchouk, A. Layadi, H. Gualous, D. Pascal, A. Koster, and S. Laval, "High-efficiency light coupling in a submicrometric silicon-on-insulator waveguide," Appl. Opt. **39,** 5773–5777 (2000).
23. J. C. Brazas and L. Li, "Analysis of input-grating couplers having finite lengths," Appl. Opt. **34,** 3786–3792 (1995).
24. R. Waldhäusl, B. Schnabel, P. Dannberg, E.-B. Kley, A. Bräuer, and W. Karthe, "Efficient coupling into polymer waveguides by gratings," Appl. Opt. **36,** 9383–9390 (1997).

25. C.-K. Kwan and G. W. Taylor, "Optimization of the parallelogrammic gating diffraction efficiency for normally incident wave," Appl. Opt. **37,** 7698–7707 (1998).
26. B. Wang, J. Jiang, and G. P. Nordin, "Compact slanted grating couplers," Opt. Express **12,** 3313–3326 (2004).
27. K. Ogawa and W. S. C. Chang, "Analysis of holographic thin film grating coupler," Appl. Opt. **12,** 2167–2171 (1973).
28. S.-D. Wu and E. N. Glytsis, "Finite-number-of-periods holographic gratings with finite-width incident beams: analysis using the finite-difference frequency-domain method," J. Opt. Soc. Am. A **19,** 2018–2029 (2002).
29. S.-D. Wu and E. N. Glytsis, "Holographic grating formation in photopolymers: analysis and experimental results based on a nonlocal diffusion model and the rigorous coupled-wave analysis," J. Opt. Soc. Am. B **20,** 1177–1188 (2003).
30. S.-D. Wu and E. N. Glytsis, "Characteristics of DuPont photopolymers for slanted holographic grating formations," J. Opt. Soc. Am. B **21,** 1722–1731 (2004).